biomimetics

MDPI

Article

Fluid-Driven Generative Design of a Passive Venturi Pump for Shower Graywater Reuse: Organic Forms, Stronger Suction and a Biomimetic Perspective

Arnaud Dujany *, Georges Husband, Baptiste Oudon, Arthur Desroche and Maxime Denis

GeNumEr, Institut Polytechnique UniLaSalle, 19 Rue Pierre Waguet, 60000 Beauvais, France
* Correspondence: arnaud.dujany@unilasalle.fr

Abstract

Reusing shower graywater for toilet flushing saves drinking water, but existing systems rely on powered components. The ShowerChiottes concept uses a passive venturi pump, fitted between the tap and the shower hose, whose jet creates a vacuum intended to lift graywater into a sealed tank. We asked whether reshaping only its suction chamber by fluid-driven generative design strengthens suction. The chamber was generated with the Fluid Path study of Autodesk Fusion 360 for three air-inlet orientations. The designs were ranked by single-phase lattice Boltzmann simulations at 6 L/min, and the initial pump and the printed design, derived from the parallel-inlet outcome, were tested at a closed air inlet. Parallel and perpendicular inlets increased an unvalidated simulated suction indicator by 25% and 22%, against 4% for an oblique inlet. At an equal low flow rate, the printed design produced four times the depression of the initial pump (890 against 225 Pa), and its suction vanished at 6.3–7.1 L/min instead of 2.0–2.7 L/min. The static lift, at most 30 cm, remains insufficient in practice. For the perpendicular inlet, the algorithm recovered the co-flowing inlet of classical jet pumps. Biological analogies, drawn only a posteriori, suggest initializing generative design with bio-inspired forms.

Keywords: fluid-driven generative design; biomimetics; computational morphogenesis; venturi pump; jet pump; graywater reuse; lattice Boltzmann method; stereolithography; design thinking

1. Introduction

Domestic water use is under growing pressure from droughts and rising prices. Graywater, the wastewater from showers, baths, hand basins and laundry, represents 50 to 80% of domestic wastewater [1], and it has long been considered a resource for non-potable urban reuse [2]. Toilet flushing, which does not require drinking-water quality, is one of its most frequently discussed applications: reusing graywater for flushing can reduce household indoor water demand by more than 20%, and a quantitative microbial risk assessment concluded that graywater from bathrooms, laundries and kitchens can be used safely for this purpose after a simple microfiltration step [3]. In a field study of an off-the-shelf graywater reuse system installed in 22 homes in Southern Ontario (Canada), the system saved about 41 L of water per household and per day [4].

Systems that bring treated graywater to the toilet are available, but they combine treatment, storage, and powered components. The field study cited above evaluated their water savings, energy use, maintenance, installation and economics, and concluded that,

Check for updates

Academic Editors: Jiao Jia, Jianxing Hu, Yi Rong and Jin Huang

Received: 22 October 2026
Revised: 9 November 2026
Accepted: 12 November 2026
Published: 17 November 2026

Copyright: © 2026 by the authors. Licensee MDPI, Basel, Switzerland. This article is an open access article distributed under the terms and conditions of the Creative Commons Attribution (CC BY) license.

with low water rates and high capital costs, subsidies would be needed to support their adoption [4]. Cost, energy supply and plumbing work are therefore potential barriers to adoption. The ShowerChiottes project explores a passive alternative: a venturi pump screwed between the tap and the shower hose, or fitted in place of the shower head. The clean-water jet creates a vacuum in a sealed tank; this depression is intended to lift graywater from the shower tray into the tank, and the tank then feeds the toilet cistern by gravity. Graywater never passes through the pump; only air does, and no energy is used other than the pressure of the water network. The device must work without electricity, without heavy plumbing work, and without changing user habits.

Venturi pumps, or jet pumps, have neither a motor nor moving parts: a primary jet accelerated in a nozzle lowers the pressure in a suction chamber and entrains a secondary fluid. Their theory is well established for liquid jets that entrain and compress a gas [5], and venturi injectors are routinely analyzed by computational fluid dynamics (CFD) and experiments [6]. Their efficiency remains modest: water–water jet pumps typically reach peak efficiencies of about 30 to 35% [7]. Their improvement has mostly relied on the parametric optimization of a fixed layout, for example, the convergent and divergent angles of venturi injectors [8], or on the shape optimization of predefined ejector profiles [9]. The layout of the suction chamber, that is, how the secondary inlet connects to the region around the nozzle and what overall shape the chamber takes, is usually fixed by the designer.

Generative design denotes computer-aided workflows in which candidate geometries are produced by an algorithm from a design space, functional objectives, and constraints, rather than drawn by the designer [10]. Its most widespread engineering form distributes material within a design domain. Rooted in the search for minimum-weight structures [11] and formalized as a material distribution problem [12,13], this approach was extended to fluid flows, where the flow domain itself is shaped to minimize the dissipated power under a constraint on the fluid volume [14–17]. Formulations based on the lattice Boltzmann method have been developed for this purpose [18,19], and the combination with additive manufacturing has allowed the experimental validation of devices with freeform internal passages [20,21]. We call this family fluid-driven generative design: the shape is generated by the flow physics under a fluid objective. Computer-aided design software has made it accessible to non-specialists, for instance through the Fluid Path study of the generative-design environment of Autodesk Fusion 360, whose objective is to minimize the pressure drop between the ports of the design space [22]. Its algorithm is not publicly documented, and this study type, released as a technology preview, has since been retired from the software [23].

Generative design is often associated with biomimetics, because its outcomes look organic and because the process itself evokes morphogenesis. Aage et al. described large-scale material-distribution design as computational morphogenesis and noted the resemblance of an optimized wing structure to the bone architecture of bird beaks [24]. Conversely, load-driven bone remodeling explains trabecular architecture as a mechanically optimal structure [25], and the growth rules of trees inspired shape and layout design methods [26,27]. For fluids, Murray's principle of minimum work balances the power needed to drive blood against the cost of blood volume [28], the same kind of trade-off as in fluid-driven generative design, which minimizes dissipation under a volume constraint [14]. Biology also offers functional analogs of a jet pump. In prairie dog burrows, the wind blowing over mounds of different shapes ventilates the burrow without any moving part [29], and ambient currents have been proposed to induce flow through sponges [30], a mechanism that in situ measurements have since qualified [31]. These parallels have limits. Biological forms are not single-objective optima [32,33], and an exactly optimal bronchial tree would be so sensitive to small geometric variations that real lungs keep a safety margin [34]. An organic

appearance is therefore not evidence of a biomimetic transfer. Following the terminology of ISO 18458 [35] and the literature on biomimetic practice and process [36,37], the present work is not biomimetic in its method: no biological system inspired the initial pump, the objective of the generative tool, its constraints, or the generated shapes, and all comparisons with biology were made a posteriori, after the design was completed. We therefore treat it as computational design whose outcome is interpreted against biological analogs; we keep these analogies separate from the design decisions actually taken (Section 4.5), and we discuss how a problem-driven biomimetic step could feed the generative process (Section 4.7). Additive manufacturing is the natural partner of both approaches, since it can build the freeform geometries they produce [38].

This study asks a focused question: can fluid-driven generative design of the suction chamber alone make a passive venturi pump draw a stronger suction? The design rationale was that a chamber with lower pressure losses, which is the objective of the tool, would draw more strongly; this rationale guided the choice of the tool but was not tested as such, since the pressure drop of the generated designs was not recorded. The pump was developed through a tooled design-thinking process [39,40] in four steps: specifications, generative design of the chamber for three air-inlet orientations, comparative lattice Boltzmann simulations [41], and stereolithography prototypes tested on a depression bench. We show that, at an equal low flow rate, the printed chamber produced four times the depression of the initial pump at a closed air inlet and moved the loss of suction from 2.0–2.7 L/min to 6.3–7.1 L/min, although the corresponding static lift remains below that required by a complete installation; that, for a perpendicular air inlet, the algorithm recovered the co-flowing secondary inlet of classical jet pumps without being instructed to; and that the printed design results from a compromise between suction, regularity and manufacturability rather than from the optimum of a single criterion. The comparison with biological systems is then made a posteriori and kept separate from these engineering results (Section 4.5).

2. Materials and Methods

2.1. A Tooled Design-Thinking Process

The work was done following a design-thinking cycle [39,40] adapted here into seven phases (identify, research, innovate, plan, create, evaluate, improve), in which generative design supported the innovation phase and 3D printing supported the creation phase (Table 1). The technical work was organized in four steps: specifications (step 1), generative design of the chamber (step 2), comparative simulation (step 3), and prototyping and bench tests (step 4). Biology was not used in any of these steps: the comparison with biological systems was made after the design was completed and is presented as an interpretation (Section 4.5).

Table 1. Phases of the tooled design-thinking process and their content in this study.

Phase	Content in This Study
Identify	Need and specifications (step 1; Section 2.2)
Research	Existing solutions and venturi effect (Section 1)
Innovate	Fluid-driven generative design of the suction chamber (step 2; Section 2.3)
Plan	Selection criteria: suction, regularity, manufacturability and use (Section 2.5)
Create	Stereolithography prototypes (step 4; Section 2.6)
Evaluate	Comparative simulation (step 3; Section 2.4), then test benches (step 4; Section 2.7)
Improve	Manual variants and final compromise (Section 3.3)

2.2. System Concept and Specifications (Step 1)

The ShowerChiottes device (Figure 1a) comprises the venturi pump, a sealed intermediate tank connected to the air inlet of the pump, a line through which graywater rises from the shower tray to the tank, and a line from the tank to the toilet cistern. The pump can be screwed onto the tap upstream of the shower hose, or fitted in place of the shower head. Only the pump was built and tested in this study. The arrangement proposed for the complete device is shown in Figure 1b, and its operating cycle has three phases. During the shower, the vent valve of the tank is closed, and the pump evacuates the air above the stored water through the air line; the resulting depression draws graywater from the tray, through a strainer and a non-return valve, into the tank. A float shut-off closes the air line when the tank is full, so that graywater cannot reach the pump, and a non-return valve on the air line prevents water from the pump chamber from entering the tank when suction breaks off. After the shower, the vent valve is opened, the tank returns to atmospheric pressure, and the non-return valve of the collection line retains the stored water. The tank, placed above the cistern, then feeds the fill valve of the cistern by gravity through a non-return valve, which also prevents water from being drawn back from the cistern line during suction; the mains supply of the cistern is kept as a back-up.

(a)



(b)

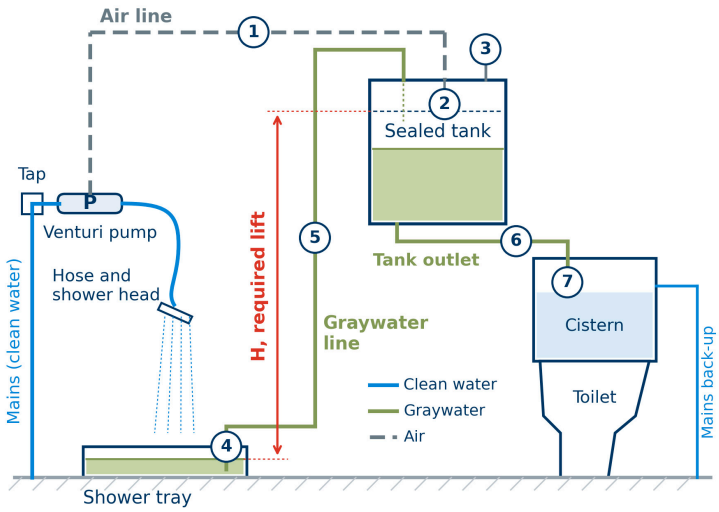


Figure 1. ShowerChiottes device. (**a**) Artist's view: the venturi pump at the shower creates a depression in the sealed tank, which lifts graywater from the shower tray; the tank then feeds the toilet cistern by gravity. (**b**) Hydraulic schematic of the arrangement proposed for the complete device (not to scale): 1, non-return valve on the air line; 2, float shut-off closing the air line when the tank is full; 3, vent valve, opened after the shower; 4, strainer; 5, non-return valve on the graywater line; 6, non-return valve on the tank outlet; 7, fill valve of the cistern; *H*, required lift. Only the pump was built and tested in this study.

The pump must therefore sustain, while drawing air, a depression at least equal to ρgH plus the friction losses of the collection line, where H is the vertical distance between the free surface in the shower tray and the maximum water level in the tank (Figure 1b). Because the tank must lie above the fill valve of the cistern, H is set by the height of the cistern. For a floor-standing toilet with a close-coupled cistern, whose fill valve typically lies 0.6 to 0.8 m above the floor, and a shower tray whose free surface lies about 0.1 m above the floor, H is at least of the order of 0.5 to 0.7 m, which requires a depression of at least about 5 to 7 kPa while air is drawn. This engineering estimate, based on typical dimensions rather than on a measured installation, is used as the reference requirement in Section 4.1.

The specifications (Table 2) were derived from the dimensions of commercial shower heads, so that the pump can be held comfortably in the hand and can fit a standard tap. Placing the pump at the shower head, as close as possible to the outlet, was preferred, because any component downstream of the pump adds pressure losses that narrow the range of flow rates at which it can operate.

Table 2. Specifications of the venturi pump.

Constraint	Requirement	Rationale
Length	<200 mm	Size of a shower head
Diameter	<70 mm	Comfortable hand grip
Mass	<650 g	Easy fitting and removal
Water connection	DN15 (nominal diameter 15 mm; 1/2 in., 21.3 mm outer diameter)	No change to the existing plumbing
Material	Watertight and mechanically resistant	Prolonged use and easy maintenance

The initial pump (Figure 2) consists of four zones: (1) a cylindrical water inlet with a DN15 internal thread (DN: nominal diameter) and a 15.02 mm bore; (2) a nozzle in which water accelerates and its pressure drops; (3) a cylindrical suction chamber surrounding the nozzle and most of the inlet duct, which receives the air through a radial inlet perpendicular to the jet; and (4) a divergent outlet that delivers the water-air mixture toward the shower. Barbed fittings on the air inlet and on the outlet allow flexible hoses to be clamped.

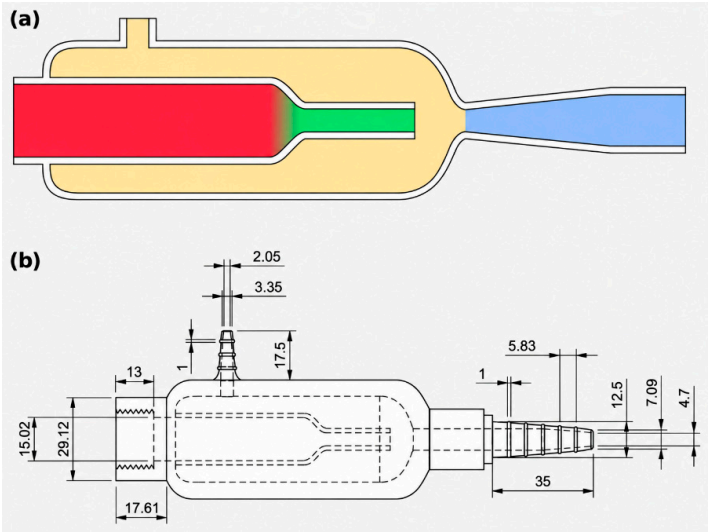


Figure 2. Initial venturi pump. (**a**) Longitudinal section showing the four zones: water inlet (red), nozzle (green), suction chamber with the air inlet at the top (yellow), and divergent outlet (blue). (**b**) Longitudinal section with the DN15 thread and barbed fittings used for testing (dimensions in mm).

2.3. Fluid-Driven Generative Design of the Suction Chamber (Step 2)

The suction chamber was generated with the Fluid Path study of the generative-design environment of Autodesk Fusion 360 (Autodesk Inc., San Francisco, CA, USA), in the release available in 2022 [22]. The initial pump was first modeled in 3D. The design domain was restricted to the suction chamber (zone 3): the water inlet, the nozzle, and the outlet were frozen as regions that the fluid could not cross, so that only the chamber was regenerated. The water inlet was placed upstream of zone 1, the air inlet on the surface of the chamber, and the outlet was set at atmospheric pressure. The study minimizes the pressure drop between the ports [22] and returns a single outcome per study. No constraint on suction was built into the tool, and the pressure drop of the outcomes was not recorded. The designs were therefore compared on suction by simulation (Section 2.4), and the expected link between lower losses and stronger suction was not tested. Before generation, the only expectation was that the outcomes would look organic, as optimized shapes often do [24]; no biological model was used to define the design domain, the objective or the constraints.

The chamber was generated for three orientations of the air inlet relative to the water jet: oblique (design A), parallel (design B), and perpendicular (design C). The orientation of the air port was thus imposed by the designer, whereas the path from the port to the region around the nozzle was left to the algorithm. Two manual variants of B were then derived: in B1, the air and water inlets were brought closer together; in B2, two lateral lobes were removed because they could trap stagnant water during use. B2 is the printed design. The simulations used the internal fluid volume only, that is, zones 1 to 4 of Figure 2a. For printing, this hollow volume was embedded in a solid body carrying the DN15 thread and the barbed fittings of Figure 2b, which were added for testing and were therefore not part of the simulated domain; the initial pump carried the same type of thread and fittings.

2.4. Comparative Lattice Boltzmann Simulations (Step 3)

The designs were compared with XFlow 2021 (Dassault Systèmes, Vélizy-Villacoublay, France), a CFD code based on the lattice Boltzmann method (LBM) [41,42]. The LBM describes the fluid through particle distribution functions defined on a lattice. At each time step, the distributions stream to the neighboring nodes and relax toward a local equilibrium through a collision operator. In its simplest, single-relaxation-time form, due to the Bhatnagar, Gross and Krook (BGK) model [43], this update reads as follows:

$$f_i(x + c_i\Delta t,\ t + \Delta t) = f_i(x,\ t) - \frac{1}{\tau}[f_i(x,\ t) - f_i^{eq}(x,\ t)] \quad (1)$$

where f_i is the distribution function along the discrete velocity $\boldsymbol{c}_i$, τ the relaxation time, related to the fluid viscosity, and f_i^{eq} the equilibrium distribution obtained from a second-order expansion of the Maxwell–Boltzmann distribution. XFlow uses the D3Q27 velocity set and, instead of the single relaxation time of Equation (1), relaxes the central moments of the distributions with multiple relaxation times, which improves Galilean invariance and numerical stability [42,44]. Distributions that meet a wall are sent back in the opposite direction, and the lattice is organized in an octree structure. Turbulence was represented by wall-modeled large eddy simulation (WMLES), with the wall-adapting local eddy-viscosity (WALE) subgrid model [45] and a non-equilibrium wall function [42]. The settings are summarized in Table 3. The single-phase free-surface configuration, the WMLES approach, and the use of the default numerical parameters are those documented for the study; the collision operator, the subgrid model, and the wall function are those implemented by XFlow 2021 for these options, as described in the literature on the solver [42,44,45], and were not read from simulation records.

Table 3. Settings of the comparative lattice Boltzmann simulations.

Item	Setting
Software and method	XFlow 2021 (Dassault Systèmes), lattice Boltzmann method (LBM); D3Q27, central-moment multiple-relaxation-time collision
Turbulence	Wall-modeled large eddy simulation (WMLES); wall-adapting local eddy-viscosity (WALE) subgrid model; non-equilibrium wall function
Phases	Free-surface model (liquid phase only); water as the only simulated fluid
Thermal model	Isothermal
Gravity	Neglected
Fluid properties	Density 1000 kg m^{-3}; dynamic viscosity 1.0×10^{-3} Pa s
Motive water flow rate	6 L/min (1.0×10^{-4} m^3 s^{-1}); Reynolds number $Re \approx 8500$ in the 15.02 mm inlet
Outlet; air inlet	Atmospheric pressure (outlet); open boundary with no imposed flow rate or pressure (air inlet)
Numerical parameters	Default settings of the software (lattice resolution and simulated duration not documented)
Hardware	Dell Precision 5820; Intel Xeon W-2155 (10 cores, 3.3 GHz); 128 GB RAM; NVIDIA Quadro RTX 5000

Three simplifications were made. First, water was the only simulated fluid. The free-surface model of XFlow computes the liquid phase only and treats any gas region as void at a prescribed pressure [46]; here, water entered the domain through both the water inlet and the air-inlet section and left through the outlet, so that the simulated configuration is, in effect, a water–water jet pump whose secondary port supplies water instead of air. This reduced the computational cost, so that several designs could be compared, but it excludes two-phase phenomena such as liquid accumulation in the chamber, the blockage of the air inlet by coalescing droplets, and the homogeneity of the outgoing water-air mixture. Second, the flow was treated as isothermal: a preliminary simulation including heat transfer (thermal conductivity 0.604 W m^{-1} K^{-1}, heat capacity 4185.5 J kg^{-1} K^{-1}) predicted a temperature rise of the order of 10^{-4} K. Third, gravity was neglected, since the orientation of the pump in use is not fixed, vertical at the tap or hand-held at the shower head. The water flow rate was set to 6 L/min, the flow rate of water-saving shower heads, which gives the Reynolds number

$$Re = \frac{4\rho Q}{\pi \mu D} \tag{2}$$

of about 8500, where ρ and μ are the density and dynamic viscosity of water, Q is the water flow rate, and $D = 15.02$ mm is the inlet bore.

Since water was the only fluid, suction was quantified by the volumetric flow rate Q_s of water computed through the air-inlet section, counted positive when water enters the chamber, that is, when the secondary port is drawn. The minimum of Q_s over the computation remained positive, between 3.30 and 4.16×10^{-5} m^3 s^{-1}, for the initial pump and for designs A, B, B1 and C, whose extrema were recorded, so that the secondary port was drawn throughout and no backflow through the air inlet occurred for these designs. For B2, only the mean and the standard deviation of Q_s were recorded, so that the absence of backflow cannot be confirmed for the printed design: a backflow would require Q_s to fall 11 standard deviations below its mean, whereas the recorded minimum of C, whose standard deviation is the same, lay 3.3 standard deviations below its mean. As neither a flow rate nor a pressure was imposed at the air-inlet section, which was left open, the pressure and the flow there result from the jet driven by the water inlet: Q_s measures how much secondary fluid the jet entrains through an open port, whereas the bench measures

the suction at a closed port, where the pressure also results from the jet and is read by the manometer (Section 2.7). Q_s is a comparative indicator used to rank the shapes, not a prediction of the air flow rate: with air about 830 times less dense than water, momentum exchange, compressibility, and the distribution of the phases differ, and no general relation links the two quantities. The lattice and time settings were the default values proposed by the software. The lattice resolution, the number of refinement levels, and the simulated duration were not documented at the time of the study and could not be recovered for this article (Section 4.6). The computed time series of Q_s was summarized by its mean and standard deviation (SD) and by its coefficient of variation (CV), the ratio of SD to the mean, and the gain of design i relative to the initial pump (subscript 0) was computed from the mean values as

$$G_i = \frac{Q_{s,i} - Q_{s,0}}{Q_{s,0}} \times 100\% \quad (3)$$

2.5. Selection Criteria

The designs were screened successively on three criteria: (i) suction, measured by the mean Q_s; (ii) regularity, measured by the SD and the CV of Q_s during the computation, since strong fluctuations indicate an irregular suction; and (iii) manufacturability and use, with a minimum wall thickness of 5 mm between the air and water inlets for mechanical strength, and no region in which water could stagnate. Each criterion was applied only to the designs retained at the previous step. The wall-thickness criterion was set after generation, when the fluid volumes were embedded in a solid body for printing; it was not imposed in the design space, although the Fluid Path study accepts obstacle regions [22] that could have enforced it. Because no lattice-sensitivity study was performed (Section 4.6), differences in mean Q_s of a few percent and differences in SD should be regarded as indicative; moreover, since the simulated duration and the averaging window are unknown, the SD and the CV describe the fluctuations over that window rather than converged statistics; their actual role in the selection is discussed in Section 3.3.

2.6. Prototyping by Stereolithography (Step 4)

The initial pump and design B2 were printed by stereolithography (SLA) on a Form 3+ printer (Formlabs Inc., Somerville, MA, USA) in White V4 resin (Formlabs), one prototype per pump. In SLA, an ultraviolet (UV) laser cures a photopolymer resin layer by layer, which yields watertight and mechanically resistant parts. After printing, the supports were removed, the uncured resin was washed off with isopropyl alcohol, and the parts were post-cured under UV. The resin met the watertightness and strength requirements of Table 2 but is not intended for long-term contact with domestic water.

2.7. Test Benches and Measured Quantities (Step 4)

Bench 1 (Figure 3a) was designed to measure both the water and the air flow rates: the outlet of the pump discharged into a sealed tank connected to a Mariotte vessel, so that the water flow rate could be obtained from the tank and the air flow rate from the volume displaced in the Mariotte vessel. It was abandoned because the pressure losses downstream of the pump were too high: above a certain water flow rate, water flowed out through the air inlet instead of air being drawn in. Only the break-off flow rates observed on this bench are reported, as preliminary observations (Section 3.4).

Bench 2 (Figure 3b) provided all the quantitative results. The pump was connected directly to a tap through its DN15 thread; the water flow rate was set with the tap, and a manometer was connected to the air inlet, which was thus closed. The supply pressure upstream of the pump was not measured directly: the manometer used for the depression

measures pressure differences between gases and cannot be connected to the water line, and the water-compatible gauges available at the laboratory could not resolve the low pressures involved, a few hundredths of a bar up to 3.4 L/min. It was derived instead from the measured flow rate and depression through the nozzle (Section 4.1), so that the measurements give access to the supply pressure, the pressure drop, the energy cost and the pressure ratio of the pumps. Since the pressure that matters for the experiment is the one at the inlet of the pump, this estimate does not depend on what is connected upstream of the pump, and the effect of the downstream configuration is contained in the measured depression. Whether a hose was attached to the outlet fitting was not documented, nor were the dates of the tests. The manometer measured the depression

$$\Delta p_s = p_{atm} - p_s \tag{4}$$

between the atmosphere and the air inlet, that is, the suction produced by the pump at zero air flow. At each operating point, the water flow rate was obtained by timing twice the collection of 1 L of water:

$$Q = \frac{60}{t_m} \tag{5}$$

with Q in L/min and t_m the mean of the two timings in s/L. The timings were read to the nearest second, which gives an uncertainty on Q of about ±1% at 1.2 L/min and up to about ±6% at 7 L/min. The depression was read twice, in mbar to the nearest 0.1 mbar (10 Pa), and results are reported as the mean ± standard deviation of the two readings ($n = 2$). The generative-design pump was tested at six flow rates between 1.15 and 7.06 L/min, and the initial pump at three flow rates between 1.20 and 2.67 L/min, in addition to the zero-flow reference. The break-off flow rate Q_b, at which the depression vanishes, was not measured directly: it lies between the highest tested flow rate with a non-zero depression and the lowest tested flow rate with a zero reading, and it is reported as this interval. A zero reading means that no depression above the 10 Pa resolution of the manometer was detected. The depression was also expressed as the equivalent static lift

$$h = \frac{\Delta p_s}{\rho g} \tag{6}$$

with $\rho = 1000$ kg m^{-3} and $g = 9.81$ m s^{-2}, that is, the height of the water column that the pump could hold at zero air flow. It is an upper bound of the lift available while air, and hence graywater, is drawn, since any air flow and the friction in the collection line reduce it.

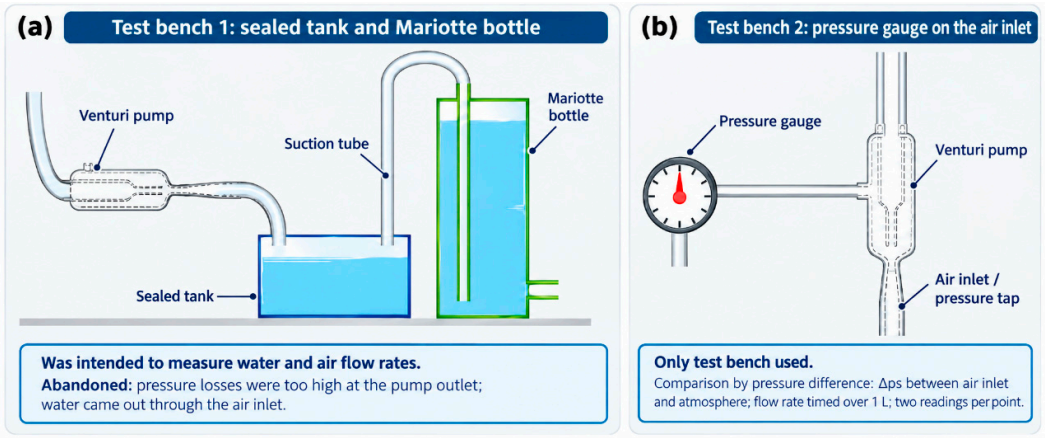


Figure 3. Test benches. (**a**) Bench 1, abandoned: the pump discharges into a sealed tank (blue) connected to a Mariotte vessel (green) to measure the water and air flow rates. (**b**) Bench 2, used for all quantitative results: a manometer is connected to the air inlet, which is thus closed.

2.8. Data Processing and Use of Generative Artificial Intelligence

Means, standard deviations, flow rates, and static lifts were computed from the raw readings, no custom code was developed for the simulations or the analysis. A generative artificial intelligence tool (Claude, Anthropic Opus 5.5 Extra, San Francisco, CA, USA) was used to assist with literature searching and reference checking, English editing of the text, drafting assistance for the revised text and the responses to the reviewers, the scripting of Figures, the drawing of the schematic of Figure 1b, and the computation of the order-of-magnitude estimates of Sections 4.1 and 4.2. All data, values, and references were checked by the authors against the raw data and the original publications.

3. Results

3.1. Generated Chamber Shapes

The three outcomes differ markedly (Figure 4). In A, with the air arriving obliquely, the chamber is compact and angular, tightly wrapped around the nozzle. In B, with the air inlet parallel to the jet, the air passage runs along the water duct and then envelops the nozzle. In C, with the air arriving from the side, the passage first descends and is then redirected along the jet. In all cases, the algorithm kept fluid where the flow circulates and removed the remaining volume, producing curved passages; B and C, in particular, show smooth transitions without sharp edges. The two manual variants of B are shown in Figure 5.

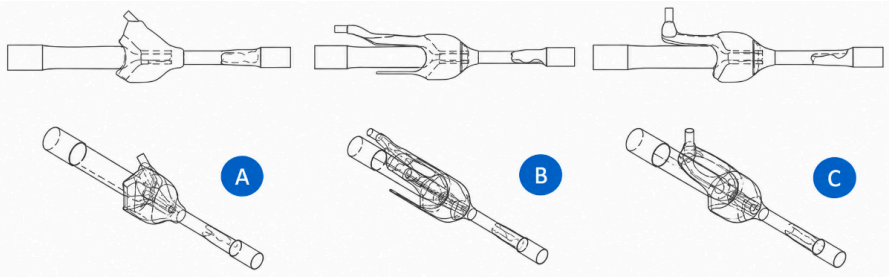


Figure 4. Suction chambers obtained by fluid-driven generative design for the three air-inlet orientations: oblique (**A**), parallel (**B**), and perpendicular (**C**). Top: side views; bottom: perspective views.

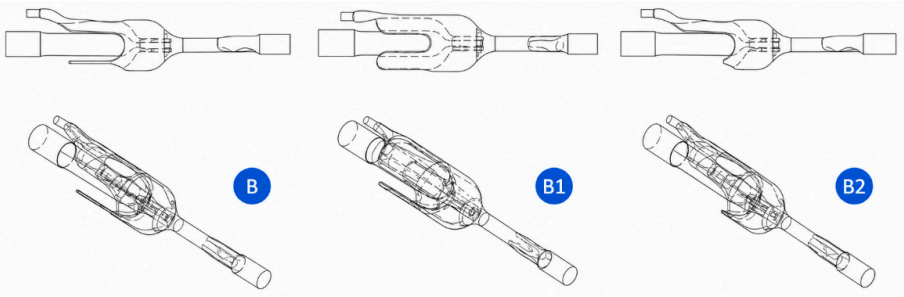


Figure 5. Design B and its manual variants: B1, with the air and water inlets brought closer together; B2, with the two lateral lobes removed to avoid stagnant water. B2 is the printed design.

B and C share a striking feature: a duct brings the air along the jet and around the nozzle, so that the secondary flow enters the mixing region co-flowing with the primary jet. This is the arrangement of classical jet pumps, in which the secondary fluid enters around the nozzle in the direction of the jet [5], whereas the initial pump admitted the air from the side, at 90° to the jet. For B, the parallel orientation of the air port, imposed as a boundary condition, already favored this layout, and the algorithm mainly shaped the passage around the nozzle. For C, the air arrived at 90° to the jet, as in the initial pump,

and the algorithm redirected it along the jet: in this case, the classical layout was recovered without any instruction to do so. For A, no duct along the jet was formed.

3.2. Simulated Suction

With water as the only fluid at 6 L/min, the initial pump gave a mean Q_s of 3.88×10^{-5} m^3 s^{-1} (Table 4, Figure 6). Designs B and C increased it by 25% and 22%, whereas A gained only 4%: with the same generative process, the simulated gain thus varied with the orientation of the air inlet. The mean of A was 16% lower than that of B and 14% lower than that of C, while B and C differed by less than 3%. B and C differed, however, in regularity. The SD of Q_s was 4.31×10^{-6} m^3 s^{-1} for C against 2.19×10^{-6} m^3 s^{-1} for B, about twice as large, and its CV was 9.1% against 4.5%. Within the B family, B1 kept the mean of B with the most regular signal (CV of 3.4%): the SD of C was 2.6 times that of B1, and the range of Q_s over the computation, from its minimum to its maximum, was 3.4 times wider for C (2.92×10^{-5} m^3 s^{-1}) than for B1 (0.85×10^{-5} m^3 s^{-1}). Removing the lobes in B2 hardly changed the mean (4.86×10^{-5} m^3 s^{-1}) but increased the fluctuations, with an SD of 4.32×10^{-6} m^3 s^{-1} and a CV of 8.9%, about twice those of B. Since no lattice-sensitivity study was performed, the differences in mean between B, B1, B2, and C, below 3%, are not resolved by the simulations; their differences in SD are indicative, and the larger differences with the initial pump and design A have not been validated either (Section 4.6).

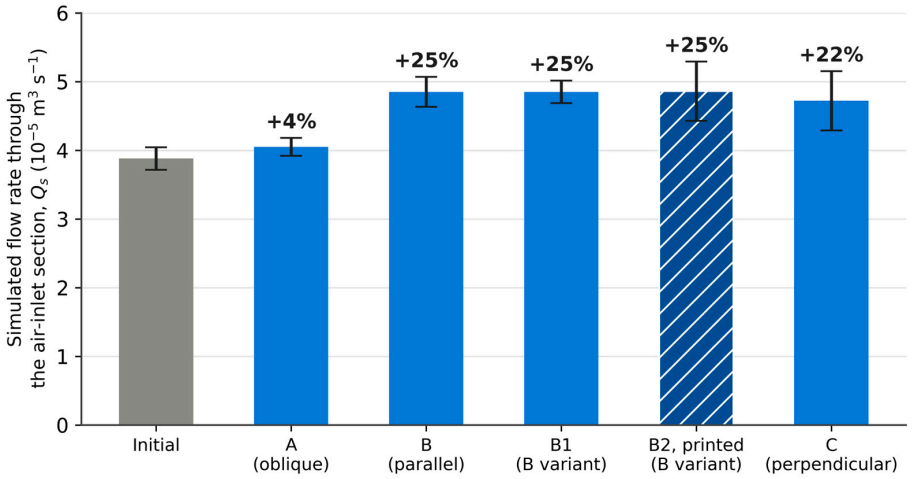


Figure 6. Mean flow rate Q_s simulated through the air-inlet section (water only, 6 L/min). Bars: Mean. Error bars: ± one standard deviation of the time series. Labels: Gain G relative to the initial pump. B2 (hatched) is the printed design.

Table 4. Flow rate Q_s simulated through the air-inlet section with water as the only fluid, at a water flow rate of 6 L/min.

Design	Air-Inlet Orientation	Mean (10^{-5} m^3 s^{-1})	SD (10^{-5} m^3 s^{-1})	CV (%)	G (%)
Initial	Perpendicular (radial)	3.88	0.164	4.2	0
A	Oblique	4.05	0.130	3.2	+4
B	Parallel	4.85	0.219	4.5	+25
B1	Parallel, inlets closer	4.85	0.165	3.4	+25
B2	Parallel, lobes removed (printed)	4.86	0.432	8.9	+25
C	Perpendicular	4.72	0.431	9.1	+22

SD: standard deviation of the time series; CV: coefficient of variation, SD divided by the mean; G: gain of the mean relative to the initial pump, Equation (3). Q_s is counted positive when water enters the chamber through the air inlet.

3.3. Selection of the Printed Design

The selection applied the criteria of Section 2.5 in turn. A was discarded for its small gain in suction (+4%). C was discarded because, although it drew almost as much as B, its suction was about twice as irregular as that of B; having been discarded at this step, it was not assessed against the third criterion. Since the averaging window of the simulations is unknown and no convergence check was made, this difference in regularity is unvalidated, and the discarding of C rests on an indicator whose meaning is uncertain. The parallel inlet also suited a pump held at the shower head, since the air line and the shower hose then leave the pump in the same direction. Within the B family, B1 was the most regular design but was discarded because the wall between the two inlets was thinner than the 5 mm minimum required for strength. B2 removed the lobes that could trap stagnant water, at the cost of fluctuations as large as those of C (CV of 8.9% against 9.1%). The regularity criterion was therefore not applied to B2 as it had been to C: at that stage, the absence of stagnant water was given precedence over regularity. In hindsight, B2 and C are equivalent on the two simulated criteria, and the choice of B2 rests on the use criterion and on the practical advantage of the parallel inlet rather than on a numerical advantage. B2 was printed as the best available compromise between suction, regularity and manufacturability rather than as the optimum of a single criterion.

3.4. Preliminary Observations on Bench 1

On bench 1, both pumps showed a break-off flow rate beyond which water flowed out through the air inlet, because the pressure losses of the downstream measuring equipment exceeded those of the air inlet. Break-off occurred at 2.8 L/min for the initial pump and at 4.6 L/min for the generative-design pump. These values depend on the downstream equipment and were not used further, but they already ranked the two pumps in the same order as the simulations.

3.5. Depression Measured on Bench 2

Table 5 and Figure 7 give the depression measured at the closed air inlet as a function of the water flow rate. For the initial pump, the highest depression, 225 ± 7 Pa, was measured at 1.20 L/min, the lowest flow rate tested; it fell to 95 ± 7 Pa at 2.03 L/min and was zero at 2.67 L/min, so that its break-off flow rate lies between 2.03 and 2.67 L/min. This pump was sampled too coarsely to locate its maximum, which may lie below 1.20 L/min or between the tested points. For the generative-design pump (B2), the depression rose from 890 ± 71 Pa at 1.15 L/min to a maximum of 2985 ± 64 Pa at 3.43 L/min, then decreased to 2470 ± 170 Pa at 5.00 L/min and 995 ± 78 Pa at 6.32 L/min, and was zero at 7.06 L/min, so that its break-off flow rate lies between 6.32 and 7.06 L/min. Both curves rose and then fell with the flow rate.

Table 6 summarizes the comparison. The like-for-like comparisons are the most robust: at an equal low flow rate (1.15 and 1.20 L/min), the depression was four times higher (890 Pa against 225 Pa), and at 2.67 L/min the initial pump no longer produced any depression, whereas the generative-design pump produced 2250 Pa. The highest measured depressions, 2985 Pa against 225 Pa, correspond to static lifts of 30.4 and 2.3 cm of water; since they were obtained at different flow rates and the maximum of the initial pump was not captured, their ratio of about 13 is only indicative. The break-off flow rate rose from between 2.03 and 2.67 L/min to between 6.32 and 7.06 L/min, a ratio between 2.4 and 3.5; the upper bound for the new pump rests on a one-second difference in the mean timings (8.5 against 9.5 s). At 6.32 L/min, close to the flow rate of a water-saving shower head, the pump still produced 995 Pa, or about 10 cm of water at zero air flow. The two timings at each point differed by at most 2 s, so that half their difference never exceeded 6% of their mean, and the two depression readings differed by at most 240 Pa.

Table 5. Depression Δp_s measured at the closed air inlet on bench 2 (raw readings, mean ± standard deviation, $n = 2$) and equivalent static lift h.

Pump	t_1 (s/L)	t_2 (s/L)	Q (L/min)	Reading 1 (Pa)	Reading 2 (Pa)	Δp_s (Pa)	h (cm)
Initial	Tap closed		0	0	0	0	0
	49	51	1.20	230	220	225 ± 7	2.3
	30	29	2.03	100	90	95 ± 7	1.0
	22	23	2.67	0	0	0	0
Generative design	Tap closed		0	0	0	0	0
	52	52	1.15	840	940	890 ± 71	9.1
	22	23	2.67	2310	2190	2250 ± 85	22.9
	17	18	3.43	3030	2940	2985 ± 64	30.4
	12	12	5.00	2350	2590	2470 ± 170	25.2
	9	10	6.32	1050	940	995 ± 78	10.1
	9	8	7.06	0	0	0	0

t_1, t_2: times to collect 1 L of water; Q: Equation (5); readings converted from mbar (1 mbar = 100 Pa); h: Equation (6). A zero reading means that no depression above the 10 Pa resolution was detected; timings were read to the nearest second.

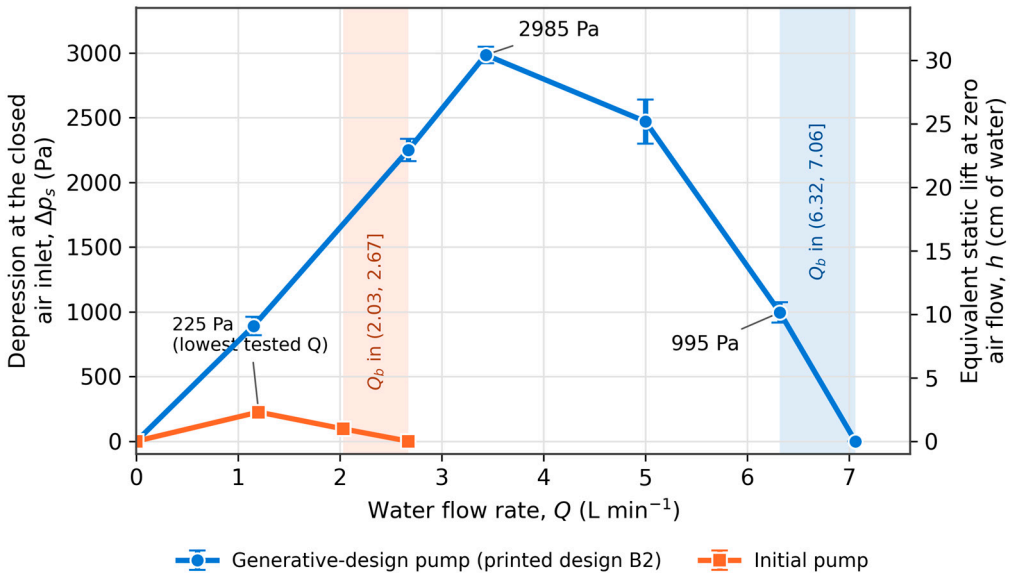


Figure 7. Depression Δp_s measured at the closed air inlet as a function of the water flow rate Q for the initial pump and the generative-design pump (B2, bench 2). Points: mean of two readings; error bars: ± one standard deviation; shaded bands: intervals containing the break-off flow rates Q_b, between the highest tested flow rate with suction and the lowest with none; right axis: equivalent static lift at zero air flow, Equation (6).

Table 6. Summary of the performance of the initial and generative-design pumps.

Indicator	Initial Pump	Generative-Design Pump	Ratio
Simulated mean Q_s at 6 L/min (10^{-5} m^3 s^{-1})	3.88	4.86 (design B2, printed)	1.25
Depression at about 1.2 L/min (Pa)	225 ± 7 (1.20 L/min)	890 ± 71 (1.15 L/min)	4.0
Highest measured depression (Pa)	225 ± 7 (1.20 L/min, lowest tested)	2985 ± 64 (3.43 L/min)	13.3 (indicative)

Table 6. *Cont.*

Indicator	Initial Pump	Generative-Design Pump	Ratio
Break-off flow rate Q_b, bench 2 (L/min)	2.03–2.67	6.32–7.06	2.4–3.5
Break-off flow rate, bench 1 (L/min)	2.8	4.6	1.6

Ratios of the highest measured values compare depressions obtained at different flow rates, and the maximum of the initial pump was not captured, so they are indicative. Break-off flow rates on bench 2 are given as intervals between the highest tested flow rate with suction and the lowest without (Section 2.7). The simulated value refers to the printed design B2.

4. Discussion

4.1. A Stronger Suction, Still Short of the System Requirement

Reshaping only the suction chamber, with the inlet, the nozzle, and the outlet unchanged, quadrupled the depression at an equal low flow rate and moved the loss of suction from 2.0–2.7 L/min to 6.3–7.1 L/min. The initial pump lost its suction below the flow rates of ordinary showers, whereas the generative-design pump still produced about 1 kPa at 6.3 L/min, the flow rate of a water-saving shower head. This answers the question raised in the Introduction for the quantity that was measured: the reshaped chamber draws a markedly stronger suction at a closed air inlet. It does not show that the device can transfer graywater. All the bench values were obtained at zero air flow and are upper bounds of the lift available while air is drawn. Even so, the highest static lift, about 30 cm at 3.4 L/min, and the 10 cm available at 6.3 L/min fall well short of the lift of 0.5 to 0.7 m estimated for a floor-standing toilet (Section 2.2). Closing this gap will require acting on the parts that were frozen here. The depression produced by a jet pump scales with the dynamic pressure of the jet [5], so that a smaller nozzle, together with a matched mixing throat and diffuser, would raise the suction at a given flow rate, at the cost of a larger pressure drop that the network pressure can supply. The characteristic of suction against air flow rate, measured with an open air inlet, is the quantity needed to size the complete device.

The supply pressure was not measured directly, but it follows from the measured flow rate. At a closed air inlet, the static pressure of the jet at the nozzle exit is the chamber pressure, so that the pressure at the pump inlet exceeds atmospheric pressure by $(1 + K_n)\rho {v_n}^2/2 - \Delta p_s$, where v_n is the mean velocity of the jet, and K_n is the loss coefficient of the nozzle. The nozzle bore, which is not dimensioned in Figure 2b, is 4.50 mm in the design file of the initial pump and was kept unchanged in the generative-design pump; its straight part is about five bores long, which gives K_n between 0.1 and 0.3 with usual contraction and friction coefficients [47]. At 6.32 L/min, this yields for the generative-design pump an inlet pressure above atmospheric pressure, and hence a pressure drop across the pump discharging to the atmosphere, of 23.1 to 27.5 kPa, a hydraulic power of 2.4 to 2.9 W drawn from the network and a shut-off pressure ratio, the depression divided by this pressure drop, of 0.036 to 0.043; at 5.00 L/min, the values are 12.6 to 15.4 kPa, 1.1 to 1.3 W and 0.16 to 0.20, and at 3.43 L/min, where its depression was highest, 4.1 to 5.4 kPa, 0.24 to 0.31 W and 0.55 to 0.73. For the initial pump, they are 0.6 to 0.8 kPa, below 0.02 W and 0.28 to 0.35 at 1.20 L/min, where its depression was highest, and 2.4 to 2.9 kPa, about 0.1 W and 0.03 to 0.04 at 2.03 L/min. Since the two pumps share the same nozzle, their inlet pressures at a given flow rate differ only by their depressions, which never differed by more than 3 kPa: the stronger suction did not require a higher supply pressure. At 1.15 L/min, the depression measured for the generative-design pump exceeds the estimated dynamic pressure of the jet, so that the inlet pressure is close to zero and not resolved. These values follow from the bench measurements and the nozzle geometry. Their uncertainty comes from the loss coefficient of the nozzle; being common to both pumps, it does not affect their

comparison, and the estimate is sufficient to evaluate their energy performance. A direct measurement would have required a water-compatible sensor resolving a few hundredths of a bar, the order of the supply pressure, up to 3.4 L/min (Section 2.7).

4.2. Simulation and Measurement Do Not Measure the Same Quantity

The simulated gain (+25%) and the measured gain (×4 at an equal flow rate) cannot be compared in magnitude, because the two indicators differ: the simulation computes a flow of water through an open air inlet, water being the only fluid, whereas the bench measures the depression at a closed air inlet. They correspond broadly to the two ends of the characteristic of a jet pump, entrainment through an open port and suction at a closed port. For a given configuration, this characteristic decreases monotonically from shut-off to free delivery [5], so that a pump with no shut-off suction cannot entrain fluid through a port open to the atmosphere. Yet the initial pump, which showed no depression at 2.67 L/min on the bench and was therefore not tested at higher flow rates, entrained water through its open port at 6 L/min in the simulation. The two configurations are therefore not equivalent. The simulation ends at the outlet of the frozen diffuser, at atmospheric pressure, whereas on the bench the flow also passes through the barbed outlet fitting, which was not simulated. This fitting is part of the printed pump and is documented in Figure 2b, where its bore narrows to 4.7 mm at its exit. Discharging freely, it requires at its inlet a pressure above atmospheric pressure of about 1.7 kPa at 2.0 L/min, 3.0 kPa at 2.7 L/min and 15 kPa at 6 L/min, that is, a loss coefficient of about 0.9 referred to its exit velocity. Most of this pressure serves to accelerate the water to its exit velocity, whose kinetic energy is then lost in the free jet, with friction estimated with the Blasius correlation adding about 10% [47]. This back-pressure is of the same order as, or larger than, the depressions measured in the chamber, at most 225 Pa for the initial pump and 2985 Pa for the generative-design pump. This order-of-magnitude estimate shows that the fitting alone imposes a back-pressure large enough to matter, but it does not test the explanation. It assumes free discharge: a hose attached to the fitting, whose presence on bench 2 was not recorded, would recover part of the exit kinetic energy but add its own friction. The secondary fluid also differs: water in the simulation and air on the bench. The two approaches agree on the ranking of the only two designs that were both simulated and tested, and both benches ranked the generative-design pump first. This agreement, on two designs and at a single simulated flow rate, is consistent with the use of the single-phase indicator to rank chamber shapes but does not establish it, and it says nothing about the relative performance of B, B2 and C, all of which were not tested. Simulations at the flow rates of maximum suction that include the outlet fittings, and two-phase simulations (Section 4.7), are needed to predict performance.

4.3. Rise and Fall of the Depression with the Flow Rate

For both pumps, the depression first increased and then decreased with the flow rate. At low flow rates, a faster jet lowers the pressure in the chamber more strongly. Beyond an optimum, the pressure in the chamber rises again, which we attribute to the pressure losses downstream of the chamber, in the outlet passage and the barbed fitting of the pump, which grow with the square of the flow rate (Section 4.2), and possibly to the choking of the mixture in the outlet; these hypotheses remain to be tested. When the chamber pressure reaches atmospheric pressure, suction vanishes, and with an open air inlet, water would flow out through it. This is the same mechanism that made bench 1 fail, where too much loss downstream forced water out through the air inlet, and it is consistent with the earlier break-off of the generative-design pump on bench 1 (4.6 L/min) than on bench 2 (between 6.32 and 7.06 L/min). It supports the choice, made in the specifications, of placing the

pump at the shower head, as close as possible to the outlet, and it points to the next design target: the outlet and the diffuser, which were kept unchanged here.

4.4. What the Algorithm Found: A Classical Layout and Organic Forms

For the perpendicular inlet, without any instruction about how the air should enter the mixing region, the generative process recovered the arrangement of classical jet pumps, in which the secondary flow enters around the nozzle and co-flows with the jet [5]. For the parallel inlet, the same arrangement largely followed from the imposed orientation of the port. Rediscovering a layout established by engineering practice lends credibility to the process. This study cannot, however, separate the two contributions: it includes no control geometry, such as the initial chamber with a parallel inlet or a simple co-flowing chamber drawn by hand, so that the specific contribution of generative shaping beyond the co-flowing layout remains unquantified. Simulating and testing such controls is the most direct way to settle this question.

The comparisons in Table 7 would separate, in part, the orientation of the air inlet from the reshaping of the chamber: at a fixed perpendicular orientation, the generated chamber C raised the simulated indicator by 22% relative to the initial chamber, whereas the oblique inlet gained only 4% with the same generative process. These differences, of 15 to 25%, are the largest of the study, but they have not been validated by a lattice-sensitivity study; the simulated duration and averaging window are unknown, and they rest on a single flow rate (Section 4.6). They are therefore reported for completeness and are not used to infer how the gain arises. The measured gain of the printed pump cannot be split either, because B2 differs from the initial pump both in the orientation of its port and in the shape of its chamber, and C was not printed.

Table 7. Comparisons available in this study and what each of them isolates.

Comparison	Held Fixed	Varied	Result
Initial pump vs. C (simulation)	Perpendicular air port; water inlet, nozzle and outlet	Chamber: initial cylindrical chamber vs. generated chamber with a co-flowing duct	+22% in mean Q_s
A vs. B vs. C (simulation)	Generative process; water inlet, nozzle and outlet	Orientation of the air port: oblique, parallel, perpendicular	+4%, +25% and +22% relative to the initial pump; co-flowing duct for B and C only
Initial pump vs. B2 (bench)	Water inlet, nozzle, outlet and test fittings	Orientation of the air port and chamber shape together	Depression ×4 at 1.15–1.20 L/min; break-off flow rate from 2.03–2.67 to 6.32–7.06 L/min
Generated vs. hand-drawn co-flowing chamber with the same port (not performed)	Orientation of the air port and co-flowing layout	Generative shaping beyond the layout	Not available: control geometry required (Section 4.6)

Q_s: flow rate simulated through the air-inlet section with water as the only fluid, at 6 L/min (Table 4). Simulated differences are not validated (Section 4.6) and are not used to infer a mechanism.

Compared with conventional co-flowing jet pumps, the contribution of the approach is not a new pumping principle. Classical jet pump analysis relates performance to the nozzle-to-throat area ratio and to the losses along the flow path [5], and the nozzle, the

mixing throat, and the diffuser were frozen here, whereas the shape of the suction chamber is usually drawn by the designer (Section 1). What the generative step contributed is a chamber in which the co-flowing arrangement was obtained automatically from an imposed port position, including one perpendicular to the jet as for C, in the form of smooth passages that stereolithography can print directly. This is useful when the position of the secondary port is constrained by the installation rather than chosen for the flow. Whether generative shaping performs better than a co-flowing chamber drawn by hand for the same port remains to be shown with the controls described above (Table 7, last row).

The outcomes also share smooth, curved passages without sharp edges, often described as organic. These forms were obtained without any bio-inspired instruction, and they could be built only because stereolithography can manufacture freeform internal passages [38].

4.5. A Biomimetic Reading, Drawn a Posteriori

The comparison with living systems must be made with care, and it was made after the design was completed: none of the analogies below informed a design decision, and Table 8 sets each of them against the corresponding design element and its actual origin. We do not claim that nature optimizes, nor that an organic appearance proves a biological analogy [32,33]. Two parallels are nevertheless instructive. The first is functional. Prairie dog burrows are ventilated by the wind, without any moving part, through the pressure differences created by the external flow over mounds of different shapes [29]. The pump performs the same function: it uses the kinetic energy of a primary flow to draw a secondary fluid out of a cavity. The analogy concerns the function only: no geometric feature of the burrow was transferred to the pump. The second concerns the selection of the final design. The bronchial tree is not exactly optimal, because an optimal tree would be so sensitive to small geometric variations that the lung keeps a safety margin [34]. Likewise, the printed design was not the optimum of a single criterion but a compromise between suction, regularity and manufacturability: the most regular variant (B1) was discarded because its wall was too thin, and a less regular one (B2) was accepted to avoid stagnant water. As in living systems, constraints other than raw performance—here, manufacturability and use—shaped the final form.

Table 8. Biological analogies discussed in this study, the corresponding design elements and their actual origin.

Biological Principle or System	Feature Shared with the Pump	Corresponding Element of This Study and Its Actual Origin	Status in This Study
Murray's principle of minimum work in vascular networks [28]	Minimum dissipation of the transported flow	Objective of the Fluid Path study, minimum pressure drop (Section 2.3): set by the tool, chosen for an engineering rationale	A posteriori analogy; hypothesis to be tested quantitatively
Wind-induced ventilation of prairie dog burrows [29]	Passive suction of a fluid from a cavity by the kinetic energy of a primary flow, without moving parts	Passive operation without electricity (Section 2.2): specification derived from the use	A posteriori functional analog; candidate model for a problem-driven approach (Section 4.7)
Safety margin of the bronchial tree [34]	Final form not the optimum of a single performance criterion	Selection of B2 (Section 3.3): manufacturability (5 mm wall) and use (no stagnant water)	A posteriori analogy; no robustness criterion was used
Computational morphogenesis and growth-based shape optimization [24–27]	Smooth, organic-looking shapes produced by an optimization or growth rule	Curved passages without sharp edges (Section 3.1): output of the tool, without bio-inspired instruction	Visual resemblance only, not evidence of a biological transfer [32,33]

All analogies were drawn after the design was completed; none of them was used as a design input.

More generally, the objective of the tool, minimizing pressure losses under geometric constraints, is of the same nature as Murray's principle of minimum work [28], which may explain why such processes produce forms that recall biological flow passages, as the morphogenetic reading of large-scale material-distribution design also suggests [24]. This remains a hypothesis. It should be tested quantitatively, for example by comparing the evolution of cross-sections or the distribution of wall shear stress in generated and biological passages, rather than by visual resemblance. The analogy concerns the objective, not a geometric law: Murray's law relates the radii of the vessels of a network to the flows they carry, most visibly at branchings, whereas each generated chamber is a single passage carrying a single secondary flow from the air port to the region around the nozzle, so that the law itself cannot be checked on it.

Table 8 shows that every design decision of this study had an engineering origin: the objective was that of the tool, passive operation was a specification of the use, and the final compromise followed from manufacturability and use. The biological analogies did not change any of these decisions. Their contribution is interpretive and prospective: Murray's principle provides a quantitative hypothesis on the generated geometries, the ventilation of burrows identifies a biological model of the same function that a problem-driven approach could analyze [37], and the safety margin of the bronchial tree suggests adding a robustness criterion to the objective, which was not done here. Turning these analogies into design inputs is the step proposed in Section 4.7.

4.6. Limitations

This study has several limitations. On the experimental side, only one prototype of each pump was tested, with two readings per point, and the initial pump was measured at three flow rates only, so that the reported standard deviations are indicative; the maximum of the initial pump was not captured, and the break-off flow rates are known only as intervals. The flow rate was set with the tap and obtained by timing with a resolution of 1 s, which limits its precision at the highest flow rates. For the generative-design pump, the break-off interval already corresponds to one second of filling time, whereas for the initial pump, finer flow rate steps and points below 1.2 L/min to locate its maximum would narrow the reported values; the conclusions are therefore stated so as to hold at either bound of the intervals. The bench tests were carried out within a student project that has ended, and the printed prototype is no longer available, so that the measurements could not be repeated or extended for this article. The supply pressure was not measured directly (Section 2.7), so the pressure drop, the pressure ratio, and the energy cost of the pumps are derived from the measured flow rates and depressions (Section 4.1); whether a hose was attached downstream and the dates of the tests were not documented, so that identical supply conditions for the two pumps cannot be guaranteed; and in use, a hose and a shower head downstream would add losses that reduce suction. The next experimental step is therefore a new prototype tested on a bench with a regulated supply, a flowmeter and a low-range pressure sensor upstream of the pump, which would allow finer flow rate steps near break-off and down to the maximum of the initial pump, a direct measurement of the supply pressure and tests with defined outlet configurations. No air flow rate was measured, so the suction available while drawing air, and hence the graywater transfer, remains unknown. On the numerical side, the simulations were single-phase, used the default parameters of the software, whose lattice and time settings were not documented, were run at a single flow rate, each WMLES computation required a long computing time, did not include the outlet fittings, and were not accompanied by a lattice-sensitivity study or a check of the statistical convergence of the mean and SD [48]; their simulated duration and averaging window are unknown, and the minimum of Q_s was not recorded for B2. The differences between B, B1, B2 and C are

therefore not resolved, and the larger differences between these designs and the initial pump or design A are unvalidated. No control geometry was simulated to separate the effect of generative shaping from that of the co-flowing layout. The Fluid Path study is proprietary; its algorithm is not documented, and it has been retired from the software [23]. To support reproducibility, the generated geometries are available from the corresponding author on request. Finally, the complete device of Figure 1b, its valves, and its operating cycle have not been built, and the durability of the printed parts, the fouling of the air line, and the quality of the stored graywater were not studied, although graywater never passes through the pump itself.

4.7. Perspective: An Augmented Design-Thinking Process

In the present process, generative design served to innovate and 3D printing to create, while biomimetics appeared only at the interpretation stage. A natural next step is to bring biology upstream, in a problem-driven biomimetic approach [37]. In the research phase, biological systems that achieve passive suction would be analyzed for the target function. In the innovation phase, generative design would be initialized with a bio-inspired shape, since its result depends on the starting geometry. 3D printing would then build the resulting organic forms directly, and the evaluation would include robustness criteria, not only performance. In short, living systems would propose, numerical optimization would refine, and 3D printing would build. The other priorities concern the physics of the pump. The blockage of the air inlet, the water leaving through the air inlet on bench 1, and the break-off of suction at high flow rates are two-phase phenomena that the present model cannot capture. A two-phase lattice Boltzmann model able to handle the water-to-air density ratio of about 830, wall wettability, and droplet coalescence is the natural next step within the same numerical framework: for instance, a color-gradient model with a multiple-relaxation-time collision operator, which remains stable at density ratios of the order of 1000 [49], combined with a wetting boundary condition [50], or a conservative phase-field formulation [51]. Such a model would give the air flow rate drawn by each design directly, instead of the comparative indicator Q_s, and it should be validated against a measured characteristic of suction against air flow rate. The nozzle, the mixing throat and the diffuser, which were frozen here, should then be designed together with the chamber.

5. Conclusions

From an engineering perspective, this study shows the following. Fluid-driven generative design of the suction chamber alone, embedded in a tooled design-thinking process and combined with lattice Boltzmann simulation and stereolithography, produced a passive venturi pump for shower graywater reuse that draws a much stronger suction at a closed air inlet than its initial design. The simulated suction indicator, which has not been validated, increased by 25% for the parallel air inlet and by 22% for the perpendicular inlet. On the bench, the depression at an equal low flow rate was multiplied by four, suction vanished between 6.3 and 7.1 L/min instead of between 2.0 and 2.7 L/min, and the highest measured depression was 2985 Pa against 225 Pa, an indicative ratio; this was obtained with no energy other than the network pressure, about 2.4 to 2.9 W of hydraulic power at 6.3 L/min, and without a higher supply pressure than for the initial pump. The corresponding static lift at zero air flow, at most 30 cm, remains below the lift required by a complete installation, so that the transfer of graywater has yet to be demonstrated. For the perpendicular inlet, the algorithm recovered the co-flowing secondary inlet of classical jet pumps without instruction; how much of the gain is due to this layout and how much to generative shaping was not determined. The printed design resulted from a compromise between suction, regularity and manufacturability.

From a biomimetic perspective, this study proposes an interpretation, not a demonstrated transfer. No biological model was used to design the pump, and the comparison with living systems was made a posteriori (Table 8). The generated passages look organic: the objective of the tool is of the same nature as Murray's principle of minimum work; the pump performs the function of wind-ventilated burrows; and the final compromise recalls the safety margin of living systems. These are analogies or hypotheses, and only the link with Murray's principle can be tested quantitatively on the generated geometries.

The next steps are a lattice-sensitivity study of the simulations, control geometries separating the effect of the layout from that of generative shaping, a new prototype tested on an instrumented bench with a regulated supply, a flowmeter and a low-range pressure sensor for direct measurements of the supply pressure at finer flow rate steps and with defined outlet configurations, two-phase modeling, the measurement of suction against air flow rate, the joint design of the nozzle, throat and diffuser and, for a biomimetic step proper, the initialization of generative design with bio-inspired forms selected through a problem-driven approach.

Author Contributions: Conceptualization, B.O. and A.D. (Arnaud Dujany); methodology, A.D. (Arthur Desroche), B.O., M.D. and A.D. (Arnaud Dujany); software, A.D. (Arthur Desroche); validation, A.D. (Arnaud Dujany); formal analysis, A.D. (Arthur Desroche), G.H. and A.D. (Arnaud Dujany); investigation, A.D. (Arthur Desroche) and A.D. (Arnaud Dujany); resources, B.O. and M.D.; data curation, G.H. and A.D. (Arnaud Dujany); writing (original draft preparation), G.H. and A.D. (Arnaud Dujany); writing (review and editing), G.H., B.O., A.D. (Arthur Desroche), M.D. and A.D. (Arnaud Dujany); visualization, A.D. (Arthur Desroche) and G.H.; supervision, A.D. (Arnaud Dujany); project administration, A.D. (Arnaud Dujany); funding acquisition, A.D. (Arnaud Dujany). All authors have read and agreed to the published version of the manuscript.

Funding: This research was funded by La Fondation Dassault Systèmes and by internal funds of Institut Polytechnique UniLaSalle.

Institutional Review Board Statement: Not applicable.

Informed Consent Statement: Not applicable.

Data Availability Statement: The original data presented in this study are included in the article: Table 5 gives all the raw bench readings and Table 4 the simulated values. The generated geometries are available on request from the corresponding author.

Acknowledgments: The authors thank Charlie Carpene (Charlie Carpene Conseil), who initiated the ShowerChiottes project, which received the Dassault Systèmes Project of the Year award in 2022, and the GéoLab of Institut Polytechnique UniLaSalle for the computing, 3D modeling, and 3D printing facilities. During the preparation of this manuscript, the authors used Claude (Anthropic; Claude Opus 5.5) for the purposes of literature searching and reference checking, English editing, drafting assistance during the revision, the scripting of Figures 6 and 7, and the drawing of Figure 1b. The authors have reviewed and edited the output and take full responsibility for the content of this publication.

Conflicts of Interest: The authors declare no conflicts of interest. The funders had no role in the design of the study; in the collection, analysis, or interpretation of data; in the writing of the manuscript; or in the decision to publish the results.

Abbreviations

The following abbreviations are used in this manuscript:

BGK	Bhatnagar–Gross–Krook (collision operator)
CFD	Computational fluid dynamics
CV	Coefficient of variation
DN	Nominal diameter
LBM	Lattice Boltzmann method

SD	Standard deviation
SLA	Stereolithography
UV	Ultraviolet
WALE	Wall-adapting local eddy viscosity
WMLES	Wall-modeled large eddy simulation

References

1. Filali, H.; Barsan, N.; Souguir, D.; Nedeff, V.; Tomozei, C.; Hachicha, M. Greywater as an alternative solution for a sustainable management of water resources: A review. *Sustainability* **2022**, *14*, 665. [CrossRef]
2. Li, F.; Wichmann, K.; Otterpohl, R. Review of the technological approaches for grey water treatment and reuses. *Sci. Total Environ.* **2009**, *407*, 3439–3449. [CrossRef] [PubMed]
3. Shi, K.-W.; Wang, C.-W.; Jiang, S.C. Quantitative microbial risk assessment of greywater on-site reuse. *Sci. Total Environ.* **2018**, *635*, 1507–1519. [CrossRef] [PubMed]
4. Craig, M.; Richman, R. Towards development of a standard methodology for testing field performance of residential greywater reuse systems: Case study of a greywater reuse system installed in 22 homes in Southern Ontario (Canada). *J. Water Reuse Desalin.* **2018**, *8*, 135–152. [CrossRef]
5. Cunningham, R.G. Gas compression with the liquid jet pump. *J. Fluids Eng.* **1974**, *96*, 203–215. [CrossRef]
6. Li, H.; Li, H.; Huang, X.; Han, Q.; Yuan, Y.; Qi, B. Numerical and experimental study on the internal flow of the venturi injector. *Processes* **2020**, *8*, 64. [CrossRef]
7. Kabaly, M.; El-Gamal, H.; Saber, E.; Afify, R. Experimental and numerical study of a water-water ejector. *J. Umm Al-Qura Univ. Eng. Archit.* **2025**, *16*, 816–826. [CrossRef]
8. Zhang, Z.; Li, Y.; Gao, J.; Tang, P.; Huang, F. Structural optimization of the venturi fertilizer applicator using head loss calculation methods. *Fluids* **2025**, *10*, 87. [CrossRef]
9. Talebiyan, M.A.; Nili-Ahmadabadi, M.; Ha, M.Y. Adjoint optimization of a supersonic ejector for under-expanded, isentropic, and over-expanded primary flow modes. *Chem. Eng. Sci.* **2024**, *292*, 119979. [CrossRef]
10. Krish, S. A practical generative design method. *Comput.-Aided Des.* **2011**, *43*, 88–100. [CrossRef]
11. Michell, A.G.M. The limits of economy of material in frame-structures. *Lond. Edinb. Dublin Philos. Mag. J. Sci.* **1904**, *8*, 589–597. [CrossRef]
12. Bendsøe, M.P.; Kikuchi, N. Generating optimal topologies in structural design using a homogenization method. *Comput. Methods Appl. Mech. Eng.* **1988**, *71*, 197–224. [CrossRef]
13. Bendsøe, M.P. Optimal shape design as a material distribution problem. *Struct. Optim.* **1989**, *1*, 193–202. [CrossRef]
14. Borrvall, T.; Petersson, J. Topology optimization of fluids in Stokes flow. *Int. J. Numer. Methods Fluids* **2003**, *41*, 77–107. [CrossRef]
15. Gersborg-Hansen, A.; Sigmund, O.; Haber, R.B. Topology optimization of channel flow problems. *Struct. Multidiscip. Optim.* **2005**, *30*, 181–192. [CrossRef]
16. Olesen, L.H.; Okkels, F.; Bruus, H. A high-level programming-language implementation of topology optimization applied to steady-state Navier-Stokes flow. *Int. J. Numer. Methods Eng.* **2006**, *65*, 975–1001. [CrossRef]
17. Alexandersen, J.; Andreasen, C.S. A review of topology optimisation for fluid-based problems. *Fluids* **2020**, *5*, 29. [CrossRef]
18. Pingen, G.; Evgrafov, A.; Maute, K. Topology optimization of flow domains using the lattice Boltzmann method. *Struct. Multidiscip. Optim.* **2007**, *34*, 507–524. [CrossRef]
19. Nørgaard, S.; Sigmund, O.; Lazarov, B. Topology optimization of unsteady flow problems using the lattice Boltzmann method. *J. Comput. Phys.* **2016**, *307*, 291–307. [CrossRef]
20. Lazarov, B.S.; Sigmund, O.; Meyer, K.E.; Alexandersen, J. Experimental validation of additively manufactured optimized shapes for passive cooling. *Appl. Energy* **2018**, *226*, 330–339. [CrossRef]
21. Yonekura, K.; Hattori, H.; Nishizu, T. Fluid topology optimization and additive manufacturing of a liquid atomizer using an extensive number of grid points. *Int. J. Adv. Manuf. Technol.* **2023**, *126*, 1799–1806. [CrossRef]
22. Houghton, H. Everything You Need to Know About Optimized Generative Design Fluid Paths. Autodesk Fusion Blog, 5 October 2021. Available online: https://www.autodesk.com/products/fusion-360/blog/de/optimized-generative-design-fluid-paths/ (accessed on 30 October 2026).
23. Patil, R. Re: Fluid Path. Autodesk Community, Fusion Design, Validate & Document Forum, 16 October 2025. Available online: https://forums.autodesk.com/t5/fusion-design-validate-document/fluid-path/m-p/14062189 (accessed on 30 October 2026).
24. Aage, N.; Andreassen, E.; Lazarov, B.S.; Sigmund, O. Giga-voxel computational morphogenesis for structural design. *Nature* **2017**, *550*, 84–86. [CrossRef] [PubMed]
25. Huiskes, R.; Ruimerman, R.; van Lenthe, G.H.; Janssen, J.D. Effects of mechanical forces on maintenance and adaptation of form in trabecular bone. *Nature* **2000**, *405*, 704–706. [CrossRef] [PubMed]

26. Mattheck, C.; Burkhardt, S. A new method of structural shape optimization based on biological growth. *Int. J. Fatigue* **1990**, *12*, 185–190. [CrossRef]
27. Baumgartner, A.; Harzheim, L.; Mattheck, C. SKO (soft kill option): The biological way to find an optimum structure topology. *Int. J. Fatigue* **1992**, *14*, 387–393. [CrossRef]
28. Murray, C.D. The physiological principle of minimum work: I. The vascular system and the cost of blood volume. *Proc. Natl. Acad. Sci. USA* **1926**, *12*, 207–214. [CrossRef] [PubMed]
29. Vogel, S.; Ellington, C.P.; Kilgore, D.L. Wind-induced ventilation of the burrow of the prairie-dog, *Cynomys ludovicianus*. *J. Comp. Physiol.* **1973**, *85*, 1–14. [CrossRef]
30. Vogel, S. Current-induced flow through living sponges in nature. *Proc. Natl. Acad. Sci. USA* **1977**, *74*, 2069–2071. [CrossRef] [PubMed]
31. Leys, S.P.; Yahel, G.; Reidenbach, M.A.; Tunnicliffe, V.; Shavit, U.; Reiswig, H.M. The sponge pump: The role of current induced flow in the design of the sponge body plan. *PLoS ONE* **2011**, *6*, e27787. [CrossRef] [PubMed]
32. Gould, S.J.; Lewontin, R.C. The spandrels of San Marco and the Panglossian paradigm: A critique of the adaptationist programme. *Proc. R. Soc. Lond. B Biol. Sci.* **1979**, *205*, 581–598. [CrossRef] [PubMed]
33. Parker, G.A.; Smith, J.M. Optimality theory in evolutionary biology. *Nature* **1990**, *348*, 27–33. [CrossRef]
34. Mauroy, B.; Filoche, M.; Weibel, E.R.; Sapoval, B. An optimal bronchial tree may be dangerous. *Nature* **2004**, *427*, 633–636. [CrossRef] [PubMed]
35. *ISO 18458:2015*; Biomimetics: Terminology, Concepts and Methodology. International Organization for Standardization: Geneva, Switzerland, 2015.
36. Vincent, J.F.V.; Bogatyreva, O.A.; Bogatyrev, N.R.; Bowyer, A.; Pahl, A.-K. Biomimetics: Its practice and theory. *J. R. Soc. Interface* **2006**, *3*, 471–482. [CrossRef] [PubMed]
37. Fayemi, P.E.; Wanieck, K.; Zollfrank, C.; Maranzana, N.; Aoussat, A. Biomimetics: Process, tools and practice. *Bioinspiration Biomim.* **2017**, *12*, 011002. [CrossRef] [PubMed]
38. du Plessis, A.; Broeckhoven, C.; Yadroitsava, I.; Yadroitsev, I.; Hands, C.H.; Kunju, R.; Bhate, D. Beautiful and functional: A review of biomimetic design in additive manufacturing. *Addit. Manuf.* **2019**, *27*, 408–427. [CrossRef]
39. Dorst, K. The core of 'design thinking' and its application. *Des. Stud.* **2011**, *32*, 521–532. [CrossRef]
40. Dym, C.L.; Agogino, A.M.; Eris, O.; Frey, D.D.; Leifer, L.J. Engineering design thinking, teaching, and learning. *J. Eng. Educ.* **2005**, *94*, 103–120. [CrossRef]
41. Chen, S.; Doolen, G.D. Lattice Boltzmann method for fluid flows. *Annu. Rev. Fluid Mech.* **1998**, *30*, 329–364. [CrossRef]
42. Chávez-Modena, M.; Martínez, J.L.; Cabello, J.A.; Ferrer, E. Simulations of aerodynamic separated flows using the lattice Boltzmann solver XFlow. *Energies* **2020**, *13*, 5146. [CrossRef]
43. Bhatnagar, P.L.; Gross, E.P.; Krook, M. A model for collision processes in gases. I. Small amplitude processes in charged and neutral one-component systems. *Phys. Rev.* **1954**, *94*, 511–525. [CrossRef]
44. Geier, M.; Greiner, A.; Korvink, J.G. A factorized central moment lattice Boltzmann method. *Eur. Phys. J. Spec. Top.* **2009**, *171*, 55–61. [CrossRef]
45. Nicoud, F.; Ducros, F. Subgrid-scale stress modelling based on the square of the velocity gradient tensor. *Flow Turbul. Combust.* **1999**, *62*, 183–200. [CrossRef]
46. Körner, C.; Thies, M.; Hofmann, T.; Thürey, N.; Rüde, U. Lattice Boltzmann model for free surface flow for modeling foaming. *J. Stat. Phys.* **2005**, *121*, 179–196. [CrossRef]
47. White, F.M. *Fluid Mechanics*, 7th ed.; McGraw-Hill: New York, NY, USA, 2011.
48. Celik, I.B.; Ghia, U.; Roache, P.J.; Freitas, C.J.; Coleman, H.; Raad, P.E. Procedure for estimation and reporting of uncertainty due to discretization in CFD applications. *J. Fluids Eng.* **2008**, *130*, 078001. [CrossRef]
49. Ba, Y.; Liu, H.; Li, Q.; Kang, Q.; Sun, J. Multiple-relaxation-time color-gradient lattice Boltzmann model for simulating two-phase flows with high density ratio. *Phys. Rev. E* **2016**, *94*, 023310. [CrossRef] [PubMed]
50. Akai, T.; Bijeljic, B.; Blunt, M.J. Wetting boundary condition for the color-gradient lattice Boltzmann method: Validation with analytical and experimental data. *Adv. Water Resour.* **2018**, *116*, 56–66. [CrossRef]
51. Fakhari, A.; Mitchell, T.; Leonardi, C.; Bolster, D. Improved locality of the phase-field lattice-Boltzmann model for immiscible fluids at high density ratios. *Phys. Rev. E* **2017**, *96*, 053301. [CrossRef] [PubMed]

Disclaimer/Publisher's Note: The statements, opinions and data contained in all publications are solely those of the individual author(s) and contributor(s) and not of MDPI and/or the editor(s). MDPI and/or the editor(s) disclaim responsibility for any injury to people or property resulting from any ideas, methods, instructions or products referred to in the content.